Journal of Engineering Research xxx (xxxx) xxx

Contents lists available at ScienceDirect

Journal of Engineering Research

journal homepage: www.journals.elsevier.com/journal-of-engineering-research

Forecasting approach of ultimate bearing capacity of underreamed anchor under local shear failure

Bin Zheng [a], Mahmoud Bayat [b,*], Yehui Shi [c], Yazhou Jiang [d], Xiangdong Qian [a], Drahomír Novák [e,f], Maosen Cao [a,*]

[a] College of Mechanics and Materials, Hohai University, Nanjing 211100, China
[b] School of Architecture, University of Texas at Arlington, Arlington, TX, USA
[c] The First Geological Brigade of the Bureau of Geology and Mineral Resources of Jiangsu, Nanjing 210041, China
[d] China Three Gorges Construction Engineering (Group) Co., Ltd, Chengdu 610041, China
[e] Institute of Structural Mechanics, Faculty of Civil Engineering, Brno University of Technology, Brno 66237, Czech Republic
[f] College of Civil and Architecture Engineering, Chuzhou University, Chuzhou, China

ARTICLE INFO

Keywords:
Underreamed anchor
End resistance model
Local shear failure

ABSTRACT

The end resistance formula in the current industry specification has parameters that are difficult to determine precisely, resulting in estimated results often does not reflect the true condition of underreamed anchor. To address this problem, based on the elucidation of load transfer law when local shear damage occurs in the soil around anchor under vertical pulling action of underreamed anchor, a model of end resistance of underreamed anchor is proposed. The model can calculate the end resistance while avoiding uncertainty of parameters of current formula. Numerical simulations and field tests show that the proposed model significantly improves the accuracy of calculating end resistance of underreamed anchor.

Introduction

Addressing precision in the analysis of underreamed anchors has wide applications. These applications include advancing the use of kinetic structures as highlighted by Afzali and Hamzehloo [1], aiding with the stability of high-rise buildings as evaluated by Shakir et al., [29], and helping optimize the design of offshore structures as detailed by Haritos [14]. Additionally, shortcomings and failure modes of underreamed anchors, such as the ones shown by Lirui [21], can be improved. Current methods used to overcome load capacity uncertainties can be minimized which can lead to more sustainable construction methods, the importance of which is highlighted by Afzali and Hamzehloo [2].

In recent decades, rock bolts have been widely used in hydraulic structure and its application in soil-nailed walled structures [4,5], tall and slender structure, deep foundation pit engineering and slope engineering. Muhammad [27] evaluated the pull-out load capacity of steel bolt using Schmidt hammer and ultrasonic pulse velocity test. The bearing capacity of the rock bolt is mainly provided by the pull-out resistance of the anchoring section, and there exists a limit to improve the bearing capacity by simply increasing the length of the anchoring section. Luo et al. [23] pointed out that with the increase of rock bolt length, the anchoring effect gradually enhances, but the improvement degree decreases gradually. Ivanovic et al. [17] pointed out that it is effective to improve the bearing capacity by increasing the length of the anchoring section within the anchorage length of 10 m, but the effect is not obvious when it exceeds 10 m.

The underreamed ground anchor technology is developed on the basis of the underreamed pile, and the advantage of it is that the bearing capacity of the rock bolt can be greatly improved by applying a small amount of material. When the ordinary rock bolt cannot provide the required bearing capacity under special conditions, the underreamed ground anchor can be selected. The researches have shown that the bearing capacity of the underreamed ground anchor is increased by 15%– 50% on average compared with the ordinary rock bolt, and the maximum is 66% [26].

Zeng et al. [35] pointed out that the bearing capacity of the underreamed ground anchor consists of three parts, namely, the side friction τ_f at the interface between the ordinary anchoring section and the soil around the anchor, the side friction τ_{fd} at the interface between the underreamed anchoring section and the soil around the anchor, and the end resistance P_D of the soil around the anchor to the underreamed end. The force diagram is shown in Fig. 1.

* Corresponding authors.
E-mail addresses: mahmoud.bayat@uta.edu, mbayat14@yahoo.com (M. Bayat), cmszhy@hhu.edu.cn (M. Cao).

https://doi.org/10.1016/j.jer.2023.12.006
Received 30 September 2023; Received in revised form 10 December 2023; Accepted 19 December 2023
Available online 22 December 2023

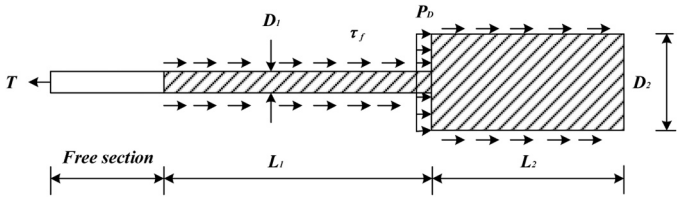

Fig. 1. Force diagram of underreamed ground anchor.

The stress process of the underreamed ground anchor is divided into three stages [32]: static earth pressure stage - transition stage - plastic zone compaction - expansion stage, among which the first stage is mainly influenced by side friction while the last two stages are mainly influenced by end resistance.

The failure modes of the underreamed ground anchor are mainly divided into three types, namely, the failure of the rod body, the cracking of the grouting body and the rod body, and the failure of the soil around the anchor [10]. Among them, the first two failure modes can be avoided by selecting reasonable structural parameters, while the third one often occurs in practical engineering.

Gao et al. [12] pointed out that uplift resistance of anchor plates were substantially influenced by anchor embedment ratio. In reinforced soil, increasing the embedment ratio greatly improved the ultimate bearing capacities of anchor plates. Zeng et al. [35] divided the failure modes of the soil around the anchor into shallow buried failure and deep buried failure according to the ratio of the buried depth of the underreamed body to the diameter of the underreamed body, which is regarded as the depth-diameter ratio, and it is pointed out that when the depth-diameter ratio is less than 5, the soil around the anchor will suffer shallow buried failure; when the depth-diameter ratio is greater than 5, the soil around the anchor will suffer deep buried failure. Hsu and Liao [15] pointed out that the shallow buried failure is the general shear failure of the soil around the anchor, and the deep buried failure is the local shear failure of the soil around the anchor. It is considered that the critical ratio of the depth to diameter ratio of these two failures is shown in Figs. 7–8. Guo [13] pointed out that the failure modes of the soil around the anchor are divided into three categories: shallow buried failure, transition failure and deep buried failure. Among them, the general shear failure occurs in the soil around the anchor under shallow buried failure and transition failure, while the local shear failure occurs in the soil around the anchor under deep buried failure. ILamparuthi and Muthukrishnaiah [16] pointed out that the general shear failure surface is approximately wavy while the local shear failure surface is approximately ellipsoidal, as shown in Fig. 2.

The main factors which influence the bearing capacity of the underreamed ground anchor are: structural parameters of the rock bolt [35], physical and mechanical parameters of the soil around the anchor [24], arrangement spacing [37], inclination of the rock bolt [9,34], grouting material [8,22].

In terms of the prediction of the ultimate bearing capacity of the underreamed ground anchor, Cheng et al., [7], Shi [30] and others put forward empirical formulas respectively. The prediction formula of bearing capacity which is more representative and adopted in the standard JGJ/T 282 [20] comes from Zeng et al. [35] in literature, and the calculation formula is:

$$T = \pi D_1 L_1 \tau_f + \pi D_2 L_2 \tau_{fd} + \frac{\pi}{4}\left(D_2^2 - D_1^2\right) P_D \tag{1}$$

T - ultimate bearing capacity of underreamed ground anchor,

D_1, D_2 - diameters of the ordinary anchoring section and the underreamed anchoring section,

L_1, L_2 - lengths of the ordinary anchoring section and the underreamed anchoring section,

τ_f, τ_{fd} - frictional resistance strength at the interface between the ordinary anchoring section as well as the underreamed anchoring section and the anchored stratum,

P_D - normal stress strength of the underreamed end face.

The end stress of the vertical rock bolt is:

$$\sigma_y = \frac{(K_0 - \xi)K_p \gamma h + 2c\sqrt{K_P}}{1 - \xi K_P} \tag{2}$$

ξ - side pressure coefficient, $\xi = (0.5\text{–}0.95)K_a$,

K_0 - static earth pressure coefficient of the soil before the underreamed end, which is based on experience $K_0 = 1\text{-}\sin(1.3\varphi)$, φ is the internal friction angle of the soil before the underreamed end,

K_p - Rankine passive earth pressure system coefficient of the soil before the underreamed end,

γ - weighted average weight of overlaying soil of the underreamed body,

h - buried depth of the underreamed body,

c - soil cohesion before the underreamed end.

The biggest defect of this formula lies in the lack of theoretical basis for the value of the lateral pressure coefficient ξ, and its value range is large, resulting in a large difference between the predicted value and the measured value. Zhao [36] pointed out that when calculating the ultimate bearing capacity of the underreamed ground anchor, the side friction and the end resistance cannot be simply added, but the weight of the side friction should be appropriately increased, which means that the enhancement coefficient $\lambda = 1.10\text{–}1.25$ should be multiplied before the side friction item. Nevertheless, the specific value of the enhancement coefficient needs to be further determined by theory and experiment.

To sum up, it is difficult to accurately determine the parameters of the end resistance formula in the current industry standard, so the estimated end resistance often cannot reflect the real situation of the underreamed anchor. In order to solve this problem, in this paper, the elucidation of load transfer law is expounded when local shear failure occurs in the soil around anchor under vertical pulling action of underreamed anchor, and a model of end resistance model of

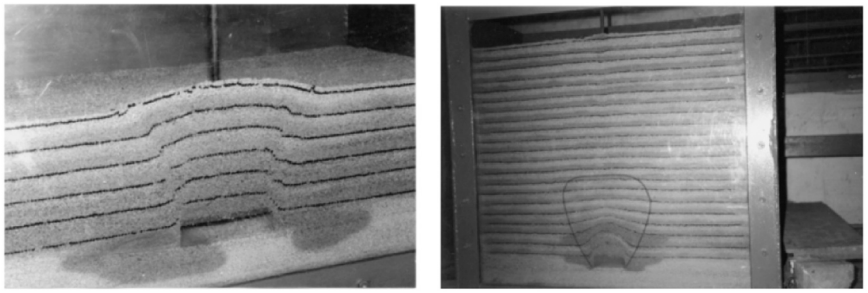

(a) general shear failure (b) local shear failure

Fig. 2. Failure modes of the soil around the anchor.

underreamed anchor is proposed. The model can be used to calculate the end resistance while avoiding uncertainty of parameters in the current formula. Numerical simulations and field tests show that the proposed model significantly improves the accuracy of calculating end resistance of underreamed anchor.

Since the frequency of general shear failure in practical engineering can be reduced by setting the minimum buried depth, this paper focuses on forecasting the ultimate bearing capacity of the underreamed ground anchor under local shear failure.

Forecasting approach of ultimate bearing capacity of underreamed anchor

The calculation methods of structural bearing capacity mainly include limit analysis method, finite element limit analysis method and limit equilibrium method [3,25,33]. The upper bound theorem of limit analysis [18,19] expresses that if any kinematically admissible velocity field (the one that satisfies the compatibility conditions, normality requirements, and velocity boundary conditions) can be considered in the problem domain, the upper bound solution can be found by equating the work done by the external loads to the internally dissipated energy, indicating that the collapse is either imminent or incipient. With the framework of the lower bound theorem of the limit analysis [28], the collapse load can be directly evaluated through a determined statically admissible stress field within the soil mass by satisfying a number of equality and inequality constraints.

As the conventional bound theorems of limit analysis are predicted on the assumption of either statically stress field or kinematically permissible velocity field, the accuracy of the results is contingent upon the soundness of such an assumption. To overcome this limitation, Sloan [31] proposed finite element limit analysis. The finite element limit analysis combines the features of conventional limit analysis and finite element method, and mutually overcomes their restrictions. Unlike the conventional bound theorems of limit analysis, the finite element limit analysis requires neither any initial assumption for statically admissible stress field nor any kinematically permissible velocity field. However, there is a big gap between the upper limit solution and the lower limit solution calculated by finite element limit analysis, so we can only simply choose the average value of the two as the standard value.

The limit equilibrium method [11] is a commonly used method to calculate the bearing capacity of structures. Its basic idea is to find out the stress state that causes stable failure of structures by changing the stress state under the premise of satisfying the equilibrium condition. At present, most of the two-dimensional structure stability analysis software used in practical engineering is based on the traditional limit equilibrium method, and many analysis results show that the limit equilibrium method has a good guiding significance for the actual structure stability evaluation, which means that the limit equilibrium method is reliable in theory.

Since the deformation zone of the soil around the anchor under local shear failure is approximately ellipsoidal, this section establishes a calculation method of end resistance based on the limit equilibrium theory according to the ellipsoidal deformation zone, and then combines it with the calculation method of side friction proposed in the standard BS 8081 [6] to establish a forecasting approach of the ultimate bearing capacity of underreamed ground anchor.

As to the geometric size of the ellipsoidal deformation zone, we make the following assumptions based on the theory of soil mechanics:

(1) The angle between the tangent line of the ellipsoidal deformation zone outside the top surface of the underreamed anchoring section and the horizontal plane is θ;
(2) The ratio of the semi-major axis b to the semi-minor axis a of the ellipsoid is t;
(3) The model is an axisymmetric model with the central axis of the underreamed ground anchor as the symmetry axis.

We take the spherical center of the ellipsoid as the coordinate origin to establish the elliptic equation, with the horizontal direction as the x axis and the vertical direction as the z axis. Taking the ellipse as the isolator for force analysis, as shown in Fig. 3. The isolator is subjected to the earth pressure of the overlaying soil, the lateral earth pressure, the self-weight of the isolator, the shear force of the soil around the anchor, and the end resistance of the underreamed anchoring section. Since the isolator is symmetrical, the lateral earth pressures in the horizontal direction offset each other.

According to the geometric boundary conditions of the isolator on the top surface of the underreamed anchoring section, the elliptic equation can be given as follows:

$$\frac{x^2}{a^2}+\frac{z^2}{b^2}=1 \tag{3}$$

$$z'_{x=R}=\tan\theta \tag{4}$$

$$b=at \tag{5}$$

The slope of the top surface of the underreamed anchoring section is:

$$z'=-\frac{b^2x}{a^2z} \tag{6}$$

$$z_{x=R}=-b\sqrt{1-\frac{R^2}{a^2}} \tag{7}$$

R - radius of the underreamed anchoring section. Put Eqs. (5)–(7) into Eq. (4), and it can be obtained that:

$$a=R\sqrt{\frac{t^2}{\tan^2\theta}+1} \tag{8}$$

$$b=Rt\sqrt{\frac{t^2}{\tan^2\theta}+1} \tag{9}$$

The height of the elliptical deformation zone h_0 is:

$$h_0=Rt\left(\frac{t}{\tan\theta}+\sqrt{\frac{t^2}{\tan^2\theta}+1}\right) \tag{10}$$

The maximum width of the elliptical deformation zone D_0 is:

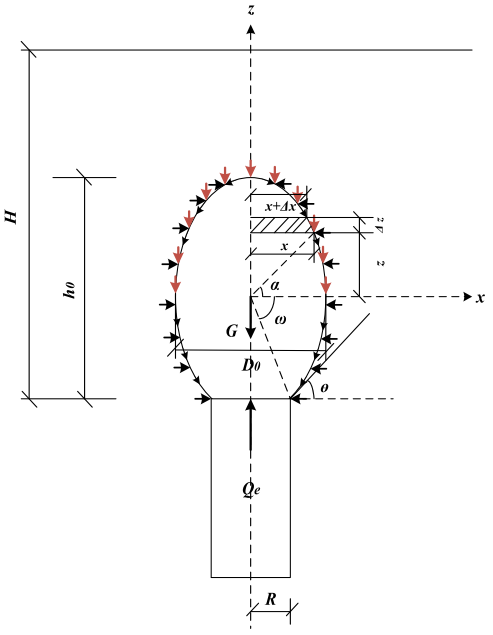

Fig. 3. Force analysis of deformation zone of the soil around the anchor.

$$D_0 = 2R\sqrt{\frac{t^2}{\tan^2\theta}+1} \tag{11}$$

We divide the elliptical micro-element into upper and lower parts for force analysis, as shown in Fig. 4. In Fig. 4(a), the normal stress acting on the external surface of the micro-element σ is:

$$\sigma = \Delta G\cos\beta + K\cdot\Delta G\cdot\sin\beta \tag{12}$$

$$\Delta G = \rho g\left(H - b\sqrt{1-\frac{R^2}{b^2}} - z - \frac{\Delta z}{2}\right) \tag{13}$$

K - soil lateral pressure coefficient,

ΔG - pressure of the overlaying soil on the surface of the micro-element,

ρ - density of the soil around the anchor,

H - buried depth of the underreamed anchoring section.

When the isolator reaches the limit equilibrium state, it can be obtained from the Mohr-Coulomb equation that:

$$\tau = \sigma\tan\varphi + c \tag{14}$$

τ - shear stress of the micro-element,

φ - internal angular friction force of the soil around the anchor,

c - cohesion of the soil around the anchor.

The resultant force of the vertical component of the upper half elliptical shear force is:

$$T_u = \int \tau\cdot\sin\beta\cdot\Delta z\cdot 2\pi(x+\Delta x) \tag{15}$$

Put Eqs. (8)–(9) and Eqs. (12)-(14) into Eq. (15), and it can be obtained that:

$$T_u = \int_0^b\left[\rho g\tan\varphi\left(H - b\sqrt{1-\frac{R^2}{a^2}} - z - \frac{\Delta z}{2}\right)(\cos\beta + K\sin\beta) + c\right] \cdot 2\pi\left(x+\frac{\Delta x}{2}\right)\cdot\Delta z\cdot\sin\beta \tag{16}$$

The elliptic parameter equation is:

$$x = a\cos\alpha \tag{17}$$

$$z = b\sin\alpha \tag{18}$$

Put Eqs. (17)-(18) into Eq. (15) as well as omit the higher-order infinitesimal terms, and then it can be obtained that:

$$T_u = 2\pi\rho gab^2\tan\varphi\left(H - b\sqrt{1-\frac{R^2}{a^2}}\right)\int_0^{2\pi}\frac{Kt - \sin\alpha\cos\alpha}{\sin^2\alpha + t^2\cos^2\alpha}\cdot\cos^2\alpha d\alpha - 2\pi\rho gab^3\tan\varphi\int_0^{2\pi}\frac{Kt - \sin\alpha\cos\alpha}{\sin^2\alpha + t^2\cos^2\alpha}\cdot\sin\alpha\cos^2\alpha d\alpha - 2\pi\rho gab^2 c\tan\varphi\int_0^{2\pi}\frac{\cos^3\alpha}{\sqrt{\sin^2\alpha + t^2\cos^2\alpha}}d\alpha \tag{19}$$

Owing to the failure to obtain the analytical solution of Eq. (19), we simplify the equation, and it can be seen that both the two integrals of the equation contain one term:

$$\frac{1}{\sqrt{\sin^2\alpha + t^2\cos^2\alpha}} \tag{20}$$

Reduce this item to:

$$\frac{1}{\sqrt{t^2\sin^2\alpha + t^2\cos^2\alpha}} = \frac{1}{t} \tag{21}$$

Enlarge this item to:

$$\frac{1}{\sqrt{\sin^2\alpha + \cos^2\alpha}} = 1 \tag{22}$$

If the difference between Eq. (21) and Eq. (22) is t times, it means that the difference between the original value and the simplified value is not more than t times. In view of the safety factors of engineering design, we adopt the reduced term Eq. (21) to make the predicted value of bearing capacity smaller. The resultant force of the vertical component of the simplified upper half elliptical shear force is:

$$T_u = \pi\rho ga^2 b\tan\varphi\left[\frac{1}{2}\left(H - b\sqrt{1-\frac{R^2}{a^2}}\right)\left(K\pi - \frac{1}{t}\right) - \frac{2}{3}bK\right] \tag{23}$$

The force analysis of the lower half of the elliptical deformation zone is shown in Fig. 4(b). Taking advantage of the same method, the resultant force of the vertical component of the lower half elliptical shear force can be obtained as follows:

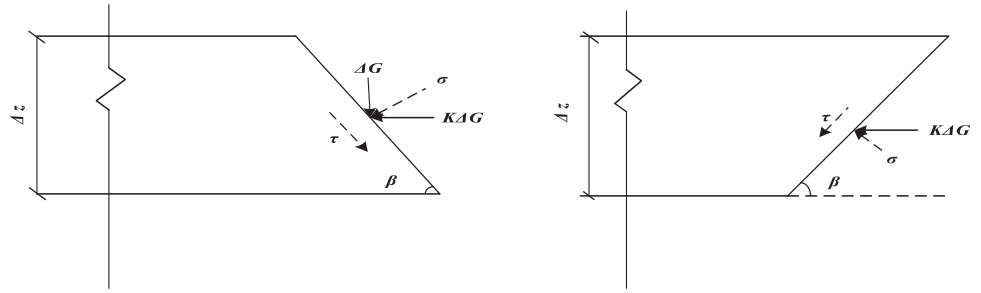

(a) the upper part (b) the lower part

Fig. 4. Force analysis of elliptical micro-element.

$$T_d = 2\pi ab\int_0^{\frac{\pi}{2}}\left[K\rho g\left(H - b\sqrt{1-\frac{R^2}{a^2}}\right)\frac{t^2\cos^4\alpha}{\sin^2\alpha + t^2\cos^2\alpha}\tan\varphi - Kb\rho g\frac{t^2\sin\alpha\cos^4\alpha}{\sin^2\alpha + t^2\cos^2\alpha}\tan\varphi + \frac{ct\cos^3\alpha}{\sqrt{\sin^2\alpha + t^2\cos^2\alpha}}\right]d\alpha \tag{24}$$

Similarly, the reduced and simplified items can be used to obtain that:

$$T_d = \frac{\pi}{2}abK\rho g\left(H - b\sqrt{1-\frac{R^2}{a^2}}\right)\tan\varphi - \frac{2}{5}\pi ab^2K\rho g\tan\varphi + \frac{4}{3}\pi abc \tag{25}$$

Hence, the resultant force of the shear force of the soil around the anchor to the isolator in the vertical direction is:

$$T = T_u + T_d = \frac{\pi}{2}ab\rho g\tan\varphi\left(H - b\sqrt{1-\frac{R^2}{a^2}}\right)\left(K + a\left(K\pi - \frac{1}{t}\right)\right) - \pi ab^2K\rho g\tan\varphi\left(\frac{2}{5} + \frac{2}{3}a\right) + \frac{4}{3}\pi abc \tag{26}$$

Since the end resistance calculation method deduced in this paper is based on the local shear failure of the soil around the anchor, the ellipsoidal deformation zone of the local shear failure mode occurs inside the soil. With the increase of the pull-out load, the size of the deformation zone gradually increases. Additionally, the compression effect on the soil around the anchor is enhanced. Thus, the lateral pressure coefficient K adopted in this paper is the passive earth pressure coefficient.

The gravity of the overlaying soil on the isolator is:

$$G = \frac{\pi}{4}D_0{}^2\cdot\rho gH \tag{27}$$

Due to the balance between the vertical resultant force of the end resistance and the shear force of the soil around the anchor to the isolator and the sum of the gravity of the overlaying soil, it can be obtained that:

$$Q_e = G + T = \pi a^2\gamma H + \frac{\pi}{2}ab\rho g\tan\varphi\left(H - b\sqrt{1-\frac{R^2}{a^2}}\right)\left(K + a\left(K\pi - \frac{1}{t}\right)\right) - \pi ab^2K\rho g\tan\varphi\left(\frac{2}{5} + \frac{2}{3}a\right) + \frac{4}{3}\pi abc \tag{28}$$

a - semi-minor axis of elliptic deformation area around anchor,

b - semi-major axis of elliptic deformation area around anchor,

t - b/a,

γ - heavy overlying soil, when the buried depth of the expanded bolt is lower than the groundwater level, the floating weight can be adopted,

ρ - soil density around anchor,

φ - internal friction angle of soil around anchor,

K - passive earth pressure coefficient,

c - cohesiveness of soil around anchor,

H - embedment depth of underreamed anchor,

R - anchorage radius of expansion body.

The bearing capacity of the underreamed ground anchor includes end resistance and side resistance. The end resistance can be obtained through Eq. (28), while the side friction is determined by the calculation method proposed in the British Industry Standard (2015), which is:

$$Q_s = Q_{sl} + Q_{sL} = c_a\pi dL_d + c_u\pi DL_D \tag{29}$$

Q_s - total side friction resistance of the underreamed ground anchor,

Q_{sl} - side friction resistance of the ordinary anchoring section,

Q_{sL} - side friction resistance of the underreamed anchoring section,

c_u - undrained shear strength of the soil layer around anchor of the underreamed anchoring section,

c_a - ultimate bond strength of the interface between the ordinary anchoring section and the soil layer around the anchor, and it generally takes 0.3–0.35c_u,

L_d - length of the ordinary anchoring section,

L_D - length of the underreamed anchoring section.

So that the ultimate bearing capacity of the underreamed ground anchor is:

$$Q = Q_e + Q_s \tag{30}$$

Method validation

In order to verify the validity of the end resistance model for forecasting the ultimate bearing capacity of the underreamed ground anchor in this paper, numerical simulation and two groups of field test data are applied for calibration in this section, namely, the field pull-out test of the underreamed ground anchor in Nanjing and Langfang.

Numerical verification

In this section, numerical simulation was performed to verify validity of the end resistance model. Basic assumptions proposed in the numerical modeling of the multi-factor, multi-parameter underreamed anchor pullout test were as follows:

(1) The material chosen for the numerical simulation was a continuous, homogeneous and isotropic elastomer;
(2) The principal structure model of the foundation model was Mohr-Coulomb model, and the shear expansion angle of soil particles was taken as 0.1°;
(3) The model was an axisymmetric model in space;
(4) The load-bearing performance of underreamed anchor was mainly based on interaction between contact surface of underreamed anchor and soil around anchor.

The pullout force in the soil around anchor was distributed axially symmetrically along the central axis, so 1/2 of the solid structure was taken for the geometric modelling. To avoid dimensional effects, the horizontal dimension of foundation model was taken as 15–25 times the diameter of underreamed anchor. For the setting of boundary conditions, all degrees of freedom at the bottom of the foundation model were constrained at the time of modeling. For each of the four sides of foundation model, constrained only the displacement in a certain horizontal direction. For example, constrained only the displacement in x-direction of side parallel to y-axis. Ground stress was applied to the entire underreamed anchor - perimeter soil model to bring its initial displacement field close to zero.

For the setting of contact stiffness of underreamed anchor - anchor perimeter soil interface, the friction coefficient of the tangential behavior penalty function was taken as 0.1–0.3 in the column of finite element software ABAQUS interaction, and the rest was the default setting of software. Linearity was chosen in the column of normal behavior stress overload, and the contact stiffness was set as follows:

$$k_n = 10\cdot\max\left(\frac{K + \frac{4}{3}G}{\Delta z_{\min}}\right) \tag{31}$$

$$K = \frac{E}{3(1-2\mu)} \tag{32}$$

$$G = \frac{E}{2(1+\mu)} \tag{33}$$

where K was the bulk modulus, G was the shear modulus, $\Delta z_{\min}$ was the minimum mesh size on the contact surface, E was the modulus of

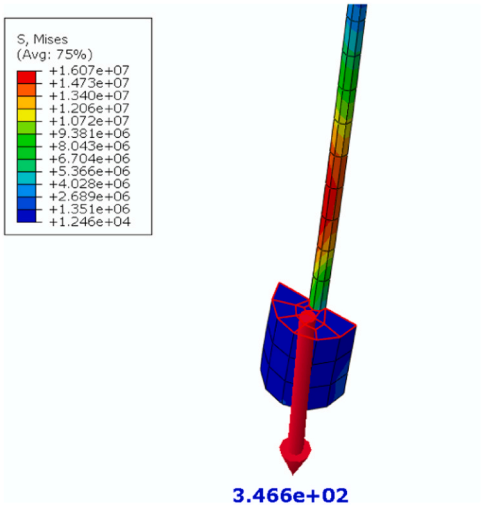

Fig. 5. End resistance of anchor segment with expanded body.

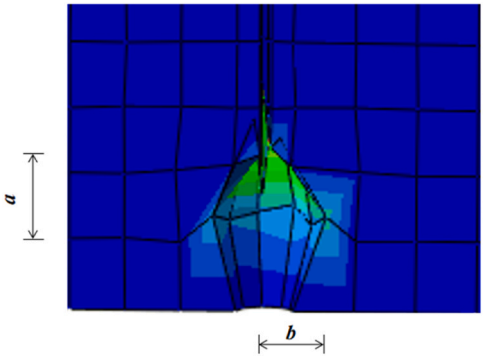

Fig. 6. Displacement nephogram of the anchorage soil.

elasticity of the foundation, and μ was the Poisson's ratio of the foundation.

The modeling parameters were as follows: number of expanded segments $n = 1$; expanded length L= 50 mm; non-expanded segment length l= 550 mm; expanded radius R= 20 mm; non-expanded radius $r = 4$ mm; peri-anchor soil density $\rho = 1473$ kg/m^3; peri-anchor soil elastic modulus $E = 2.5 \times 10^7$ Pa; peri-anchor soil Poisson's ratio $\mu = 0.3$; peri-anchor soil cohesion c= 3000 Pa; friction angle of peri-anchor soil $\varphi = 28°$; passive lateral pressure coefficient of peri-anchor soil K= 0.25; modulus of elasticity of expanded anchorage section $E = 2.8 \times 10^8$ Pa; Poisson's ration of expanded anchorage section $\mu = 0.22$; density of expanded anchorage section $\rho = 2360$ kg/m^3; modulus of elasticity of non-expanded anchorage section $E = 2.05 \times 10^{11}$ Pa; Poisson's ratio of non-expanded anchorage section $\mu = 0.27$; density of non-expanded anchorage section $\rho = 7850$ kg/m^3.

When load was 500 N, the end resistance of expanded anchorage section was 347 N, as shown in Fig. 5. Due to the symmetric modeling, actual simulated value of end resistance was 694 N. The soil damage area around anchor was semi-elliptical, as shown in Fig. 6. Based on the set grid size, half- length axis a of the anchor perimeter soil damage zone was calculated to be 0.135 m, and half-short axis b was 0.0675 m. Substituting the values of semi-long axis a, semi-short axis b and modeling parameters into Eq. (28), the theoretical value of end resistance was 636 N. The error between simulation and model value was 8.4%, which met requirements of engineering specifications.

Demonstration case 1

In this section, the reliability of end resistance model was verified through Nanjing field tests [13]. The working conditions for field test were: cohesion of the soil around anchor is c= 10kPa, internal friction angle is $\varphi = 14.3°$, soil weight is γ'= 7.7 kN/m3, burial depth H= 12 m, diameter of underreamed anchorage section is D= 0.8 m, length of underreamed anchor section is L_D= 2 m, diameter of ordinary anchorage section is d= 0.2 m. The calculated values of end resistance Q_e and side friction resistance Q_s for this condition could be obtained by Eqs. (28)-(29), and the results were listed in Table 1.

When end resistance and side friction resistance were known, the ultimate bearing capacity of underreamed anchor could be derived from Eq. (30) as 454.1 kN. Field test measured value was 450 kN, and the relative error was 0.9%, which met requirement of engineering specification. Lateral pressure coefficient ξ in Eq. (2) is the lateral pressure coefficient reflecting crowding effect of soil when expanded anchorage section is displaced forward, which can be taken as (0.5–0.9)K_a for non-prestressed anchors, and K_a is the main moving soil stress coefficient. ξ is related to the strength of soil at the front end of expended anchorage section. The upper limit should be taken for clayey soils with good strength and denser sandy soils, and the lower limit should be taken for soils with lower strength. Based on Eq. (2), the interval of end resistance Q_e could be obtained as 94–280 kN. Since expended anchorage section in the field test is buried in silty clay with low strength, ξ was taken as 0.6K_a and the end resistance Q_e was 106 kN. Standard JGJ/T 282 [20] stipulates that average side friction resistance of common anchorage section and expanded anchor section in silty soil was 16–20kPa, and this paper took 20kPa, so the side friction resistance of common anchorage section and expanded anchorage section was 100 kN, then the ultimate bearing capacity of expanded anchor was 357 kN, and the relative error with field measured value is − 21%. The absolute value of relative error was higher than that of expanded anchor limit bearing capacity calculation method established in this paper..

Table 1
Calculation results of underreamed anchors in Field test 1.

Underreamed anchor area	Shear strength c_u (kPa)	Side friction resistance Q_s (kN)	End resistance Q_e (kN)
Ordinary anchorage section	18.9	42.7	-
Expanded anchorage section	29.2	146.8	264.6

Table 2
The geometric parameters of the capsule-type underreamed anchor in Langfang test site.

Group	Underreamed anchor length L_D [m]	Ordinary anchor length L_d [m]	Underreamed anchor diameter D [mm]	Ordinary anchor diameter d [mm]
1	3.0	12	800	180
2	1.5	13.5		
3	3.0	18.0	700	
4	1.5	19.5		

Table 3
Physical and mechanical parameters of the soil around the anchor in Langfang test site.

Buried depth H [mm]	Internal friction angle ψ [°]	Cohesion c [kPa]	Weight γ [kN/m^3]	Soil lateral pressure coefficient k	Shear strength τ [kPa]
4.2	18.2	10	8.7	0.69	14.13
5.7	9.5	25	10.1	0.84	31.16
8.1	20.0	8	8.6	0.66	22.85
9.3	9.5	25	10.1	0.84	35.95
10.4	22.3	8	10	0.62	30.89
17.1	10.6	26	10.4	0.82	45.89
19.5	11.6	24	10.5	0.80	53.14
21	11.6	24	10.5	0.80	56.49

Table 4
Calculation results of ultimate bearing capacity of on-site pull-out test of underreamed anchor in Langfang.

Group	End resistance Q_e [kN]	Side friction Q_s [kN]	Predicted value of ultimate bearing capacity Q [kN]	Measured value Q' [kN]	Error e (%)
1	269	399	668	710	-5.9
2	329	237	566	589	-3.9
3	524	474	998	1138	-12.3
4	631	300	931	1045	-10.9

Demonstration case 2

In the field pull-out test of underreamed ground anchor in Langfang [13], a total of 4 groups of 8 capsule-type underreamed ground anchors were applied for ultimate pull-out test. The geometric parameters of the rock bolts were listed in Table 3. Soil around anchor was mainly powdered clay and the physical and mechanical parameters of the soil were listed in Table 3.

Eqs. (28)-(29) were taken to calculate the end resistance and side friction of 8 underreamed ground anchors respectively. The bearing capacity values of the two underreamed ground anchors in the same group were averaged and compared with the measured values. The calculation results were listed in Table 4. The error range between calculated and measured ultimate bearing capacity values of eight underreamed anchors was 3.9%– 12.3%, which met requirements of engineering specifications.

Discussion

From the comparison results of the demonstration cases in Section 3, it can be observed that the method proposed in this paper can better forecast the ultimate bearing capacity of the vertical underreamed ground anchor under local shear failure owing to the prediction results with small error, which are all less than 25%. It turns out to be more accurate than the results obtained by the standard JGJ/T 282 [20]. The advantage of this method is that the physical meaning of the parameters in the proposed formula is clear. When the geometric parameters of the underreamed ground anchor and the physical and mechanical parameters of the soil around the anchor are known, the formula can be utilized to obtain the ultimate bearing capacity of the underreamed ground anchor, providing a certain reference for the design of the underreamed ground anchor in the practical engineering.

Conclusions

In this paper, the end resistance model of underreamed anchors subjected to local shear damage of soil around anchor by vertical pulling is proposed. Based on elucidation of load transfer law when local shear damage occurs in the soil around anchor under vertical pulling action of underreamed anchor, a model of end resistance of underreamed anchor is proposed. The parameters of model can be precisely determined, solving the problem that parameters of end resistance formula in the current industry specification are difficult to determine. The end resistance model was experimentally verified to have higher calculation accuracy than existing methods. The numerical simulation error was 8.4%, error of test 1 was 0.9%, error range between calculated and measured ultimate bearing capacity values of eight underreamed anchors in test 2 was 3.9%– 12.3%, which significantly exceeded specification calculation accuracy. In the future research, we will further explore the forecasting approach of the ultimate bearing capacity of the underreamed ground anchor with different inclination angles.

Declaration of Competing Interest

The authors declare that they have no known competing financial interests or personal relationships that could have appeared to influence the work reported in this paper.

Acknowledgements

The authors are grateful for the Fundamental Research Funds for the Central Universities [No. B220204002], the International Science & Technology Cooperation Project of Jiangsu Province (BZ2022010), the Jiangsu-Czech Bilateral Co-funding R&D Project (No. BZ2023011), and "The Belt and Road" Innovative Talents Exchange Foreign Experts Project (No. DL2023019001L).

References

[1] N. Afzali, S. Hamzehloo, Kinetic, an innovative approach in contemporary architecture, 5th Int. Conf. Mod. Res. Civ. Eng. Archit., Urban Dev. Singap. Vol. 5 (2016).
[2] N. Afzali, S. Hamzehloo, Evaluating the role of recycling materials in construction industry (case study: city of Tehran), J. Environ. Friendly Mater. 2 (2) (2018) 49–58.
[3] S. Aroni Hesari, S. Javankhoshdel, M. Payan, R. Jamshidi Chenari, Pseudo-static internal stability analysis of geosynthetic-reinforced earth slopes using horizontal slices method, Geomech. Geoengin. 17 (5) (2022) 1417–1442.
[4] M. Bayat, M. Bayat, M. Bayat, Data-driven modeling of optimal intensity measure of soil-nailed wall structures, Struct. Eng. Mech. 86 (1) (2023) 85.
[5] M. Bayat, A. Emadi, A.H. Kosariyeh, M. Kia, M. Bayat, Collapse fragility analysis of the soil nail walls with shotcrete concrete layers, Comput. Concr. 29 (5) (2022) 279–283.
[6] BS 8081, British Standard Code of Practice for Ground Anchorages, British Standard Institute; BSI Standard Limited,, London, UK, 2015.
[7] L.K. Cheng, J.L. Fan, J. Han, J.P. Xu, Geotechnical Anchorage, China Architecture & Building Press, Beijing, China, 2003.
[8] Y.L. Du, G.R. Feng, H.P. Kang, Y.J. Zhang, X.H. Zhang, Effect of steel fiber frout on the mechanical performance and failure characteristics of fully grouted bolts, Structures 33 (2021) 1096–1106, https://doi.org/10.1016/j.istruc.2021.05.013.
[9] L. Erion, P. Erion, A pioneer in-situ investigation on the bearing capacity and failure causes of real scale fully grouted rockbolts, Constr. Build. Mater. 310 (2021), 124826, https://doi.org/10.1016/j.conbuildmat.2021.124826.
[10] G.Y. Fu, R. Deo, J. Ji, J. Kodikara, Failure assessment of reinforced rock slopes subjected to bolt corrosion considering correlated multiple failure modes, Comput. Geotech. 132 (2021), 104029, https://doi.org/10.1016/j.compgeo.2021.104029.

[11] Y.F. Gao, D. Wang, F. Zhang, Current research and prospects of 3D earth slope stability analysis methods, J. Hohai Univ. (Nat. Sci.) 43 (5) (2015) 456–464, https://doi.org/10.3876/j.issn.1000-1980.2015.05.010.
[12] Y.X. Gao, H.H. Zhu, Y.F. Ni, C. Wei, B. Shi, Experimental study on uplift behavior of shallow anchor plates in geogrid-reinforced soil, Geotext. Geomembr. 50 (5) (2022) 994–1003, https://doi.org/10.1016/j.geotexmem.2022.06.006.
[13] G. Guo, Study on bearing mechanism and ultimate bearing capacity prediction of expanded bolt, Ph. D. Diss., Harbin Inst. Technol., Harbin, China (2019).
[14] N. Haritos, Introduction to the analysis and design of offshore structures– an overview, Electron. J. Struct. Eng. (1) (2007) 55–65, https://doi.org/10.56748/ejse.651.
[15] S.T. Hsu, H.J. Liao, "Uplift behavior of cylindrical anchors in sand", Can. Geotech. J. 35 (1) (1998) 70–80, https://doi.org/10.1139/t97-067.
[16] K. ILamparuthi, K. Muthukrishnaiah, Anchors in sand bed: delineation of rupture surface, Ocean Eng. 26 (12) (1999) 1249–1273, https://doi.org/10.1016/S0029-8018(98)00034-1.
[17] A. Ivanovic, A. Starkey, R.D. Neilson, A.A. Rodger, The influence of load on the frequence response of rock bolt anchorage, Adv. Eng. Softw. 34 (2003) 697–705, https://doi.org/10.1016/S0965-9978(03)00099-1.
[18] A. Izadi, L.A. Nalkiashari, M. Payan, R.J. Chenari, Bearing capacity of shallow strip foundations on reinforced soil subjected to combined loading using upper bound theorem of finite element limit analysis and second-order cone programming, Comput. Geotech. 160 (2023), 105550.
[19] A. Izadi, L.A. Nalkiashari, M. Payan, R.J. Chenari, "Bearing capacity of shallow strip foundations on reinforced soil subjected to combined loading using upper bound theorem of finite element limit analysis and second-order cone programming", *Comput. Geotech.* 160 (2023), 105550 https://doi.org/10.1016/j.compgeo.2023.105550.
[20] JGJ/T 282, Technical Specification for High Pressure Jet Enlarged Bolt, China Architecture & Building Press, Beijing, China, 2012.
[21] L. Lirui, Discussion on mechanical advantage and anti-floating stability of under-reamed ground anchorage with capsule, 2nd Int. Conf. Urban Eng. Manag. Sci. (ICUEMS), Sanya, China (2021) 237–241, https://doi.org/10.1109/ICUEMS52408.2021.00058.
[22] P. Liu, S.S. Xie, L. Liu, Z.H. Zheng, N. Zhang, S.S. He, Y.Y. Wu, W. Xu, Y. Chen, Y. C. Kuang, Z.W. Yu, Experimental study on bonding strength between high-strength bolt and cement-based grouting material, J. Mater. Res. Technol. -JMRT 19 (2022) 2191–2203, https://doi.org/10.1016/j.jmrt.2022.05.173.
[23] Y.B. Luo, Z. Shi, C.W. Wang, J.X. Chen, W.W. Liu, Y. Li, Y.F. Wu, Mechanical properties of rock bolt and analysis for the full-process of sliding failure based on rock mass absolute displacement, J. Traffic Transp. Eng. -Engl.. Ed. 9 (3) (2022) 490–506, https://doi.org/10.1016/j.jtte.2020.11.001.
[24] S.Q. Ma, J. Nemcik, N. Aziz, An analytical model of fully grouted rock bolts subjected to tensile load, Constr. Build. Mater. 49 (2013) 519–526, https://doi.org/10.1016/j.conbuildmat.2013.08.084.
[25] S.P. Maghferati, R.J. Chenari, S.H. Lajevardi, M. Payan, S.M. Mirhosseini, Seismic combined bearing capacity of strip footings on partially saturated soils using lower bound theorem of finite element limit analysis and second-order cone programming, Comput. Geotech. 157 (2023), 105327.
[26] S.B. Mickovski, A.R. Ennosl, Model and whole-plant studies on the anchorage capabilities of bulbs, Plant Soil 255 (2) (2003) 641–652, https://doi.org/10.1023/A:1026007229517.
[27] S. Muhammad, Evaluating the pull-out load capacity of steel bolt using Schmidt hammer and ultrasonic pulse velocity test, Struct. Eng. Mech. 65 (5) (2018) 601–609, https://doi.org/10.12989/sem.2018.65.5.601.
[28] M. Payan, H. Fathipour, M. Hosseini, R.J. Chenari, J.S. Shiau, Lower bound finite element limit analysis of geo-structures with non-associated flow rule, Comput. Geotech. 147 (2022), 104803, https://doi.org/10.1016/j.compgeo.2022.104803.
[29] I. Shakir, M.A. Jasim, S.S. Weli, High rise buildings: design, analysis, and safety: an overview, Int. J. Archit., Eng., Technol. 8 (2021) 1–13.
[30] S. Shi, Research on anchoring mechanism of bolts under pull-out load, Ma. Eng. Diss., Lanzhou Univ., Lanzhou, China (2012).
[31] S. Sloan, Lower bound limit analysis using finite elements and linear programming, Int. J. Numer. Anal. Meth. Geomech. 12 (1988) 61–77, https://doi.org/10.1016/0148-9062(88)91670-1.
[32] B.J. Sun, Q.W. Liu, W.T. Li, X.Z. Yang, B. Yang, T.C. Li, Numerical implementation of rock bolts with yield and fracture behavior under tensile-shear load, Eng. Fail. Anal. 139 (2022), 106462, https://doi.org/10.1016/j.engfailanal.2022.106462.
[33] M.A. Tavakoli, H. Fathipour, M. Payan, R.J. Chenari, H. Ahmadi, Seismic bearing capacity of shallow foundations subjected to inclined and eccentric loading using modified pseudo-dynamic method, Transp. Geotech. (2023), 100979.
[34] S.B. Yu, R.S. Merifield, A.V. Lyamin, X.D. Fu, Kinematic limit analysis of pullout capacity for plate anchors in sand slopes, Struct. Eng. Mech. 51 (4) (2014) 565–579, https://doi.org/10.12989/sem.2014.51.4.565.
[35] Q.Y. Zeng, X.Y. Yang, C.Y. Yang, Mechanical mechanism and calculation method of enlarged head bolt, Rock. Soil Mech. 31 (5) (2010) 1359–1368, https://doi.org/10.16285/j.rsm.2010.05.037.
[36] H.F. Zhao, Research on pull-out test of enlarged head bolt, Ma. Eng. Diss., Zhengzhou Univ., Zhengzhou, China (2012).
[37] Y.M. Zhao, M.J. Yang, Pull-out behavior of an imperfectly bonded anchor system, Int. J. Rock. Mech. Min. Sci. 48 (3) (2011) 469–475, https://doi.org/10.1016/j.ijrmms.2010.09.011.